THE ASTROPHYSICAL JOURNAL, 535:L33–L37, 2000 May 20

IMPULSIVE AND VARYING INJECTION IN GAMMA-RAY BURST AFTERGLOWS

RE'EM SARI[1] AND PETER MÉSZÁROS[1,2]

Received 2000 February 25; accepted 2000 April 11; published 2000 May 30

ABSTRACT

The standard model of gamma-ray burst afterglows is based on synchrotron radiation from a blast wave produced when the relativistic ejecta encounters the surrounding medium. We reanalyze the refreshed shock scenario, in which slower material catches up with the decelerating ejecta and reenergizes it. This energization can be done either continuously or in discrete episodes. We show that such a scenario has two important implications. First, there is an additional component coming from the reverse shock that goes into the energizing ejecta. This persists for as long as the reenergization itself, which could extend for up to days or longer. We find that during this time the overall spectral peak is found at the characteristic frequency of the reverse shock. Second, if the injection is continuous, the dynamics will be different from that in constant energy evolution and will cause a slower decline of the observed fluxes. A simple test of the continuously refreshed scenario is that it predicts a spectral maximum in the far-infrared or millimeter range after a few days.

Subject headings: gamma rays: bursts — hydrodynamics — radiation mechanisms: nonthermal — shock waves

1. INTRODUCTION

The standard model for gamma-ray burst (GRB) afterglows assumes that relativistic material is decelerating on account of interaction with the surrounding medium. A shock wave is formed, heating the surrounding matter to relativistic temperatures. It is assumed that both magnetic fields and accelerated electrons acquire an energy density that is a significant fraction of the equipartition value. In the simplest case, which will be referred to as the standard scenario, a single value of the energy and the bulk Lorentz factor is injected either as delta or as a top-hat function, of duration short with respect to the afterglow. The total energy is fixed in time and equals the initial energy of the explosion.

Slower moving material is essential to models that use density gradients as a means of acceleration. Actually, in this mechanism, most of the system's energy is carried by the slower material. This scenario overcomes the need for a clean environment. The fact that one now needs a substantially higher energy input can be addressed by a very energetic source such as a massive star. A similar situation exists in some cases of supernovae. When a shock wave propagating through the envelope of the star arrives at the edge, it accelerates, and higher and higher velocities are being imparted to a smaller fraction of the mass.

In GRB afterglows, if such slower material with significant energy is ejected, it will affect the evolution in two major ways: first, the system becomes more energetic as time passes (refreshed shock scenario), therefore the temporal decay of the afterglow will be slower (Rees & Mészáros 1998). Second, since the reverse shock will last for as long as the energy supply continues, it adds an additional long-living (reverse) emission component, typically at low frequencies. The emission from such a reverse shock was considered by Kumar & Piran (1999) for the discrete injection case. Accurate observations of the afterglow temporal decay or good spectral sampling, especially at radio to millimeter frequencies, may reveal both of these features or constrain the possibility of additional energy injection.

[1] Theoretical Astrophysics 130-33, California Institute of Technology, Pasadena, CA 91125.

[2] Also at Institute for Advanced Study, Olden Lane, Princeton, NJ and Pennsylvania State University, 525 Davey Laboratory, University Park, PA.

2. DYNAMICS

We assume that the source ejects a range of Lorentz factors for which a mass of $M(>\gamma) \propto \gamma^{-s}$ is moving with Lorentz factors greater than γ. All masses are ejected at essentially the same time (i.e., over a period that is much shorter than the afterglow timescales). The energy associated with that mass is $\gamma Mc^2 \propto \gamma^{-s+1}$. This is valid only for $s > 1$, where for $s < 1$ the energy above any Lorentz factor is constant, since it is concentrated near the highest Lorentz factor. We normalize this proportionality using the initial Lorentz factor γ_0 and the initial energy content, which is about the "burst" energy E_0,

$$E(>\gamma) \sim E_0(\gamma/\gamma_0)^{-s+1}, \tag{1}$$

down to some value $\gamma_{\min} \leq \gamma_0$. This tilted top-hat injection leads to a "refreshed" shock scenario (Rees & Mészáros 1998), in contrast to the standard straight top-hat or delta function model with a monoenergetic E_0 and a single value γ_0. Although γ_0 and E_0 are free parameters, we have lower limits on $\gamma_0 \geq 100$ to avoid pair creation during the GRB itself, and we have an estimate of the initial energy E_0 from the energy seen in the burst. The actual value of γ_0 can be obtained from the onset time of the afterglow or from the reverse shock initial frequency. This scenario is related to the Fenimore & Ramirez-Ruiz (1999) model, in which a wind with near-steady γ impacts on a decelerating "wall" produced by the outermost shells of material which first make contact with the exterior gas. The refreshed shock scenario envisages an "engine" duration which is instantaneous compared to the deceleration time, whereas the latter scenario assumes that the wind duration is longer than the initial deceleration time. However, if the engine produced a wind whose Lorentz factor decreased with time, the net effect could be rather similar to the refreshed shock.

The low Lorentz factor mass will catch up with the high Lorentz factor mass only when the latter has decelerated to a comparable Lorentz factor. At that time, the shocked material (both reverse and forward shock) has a Lorentz factor γ sat-

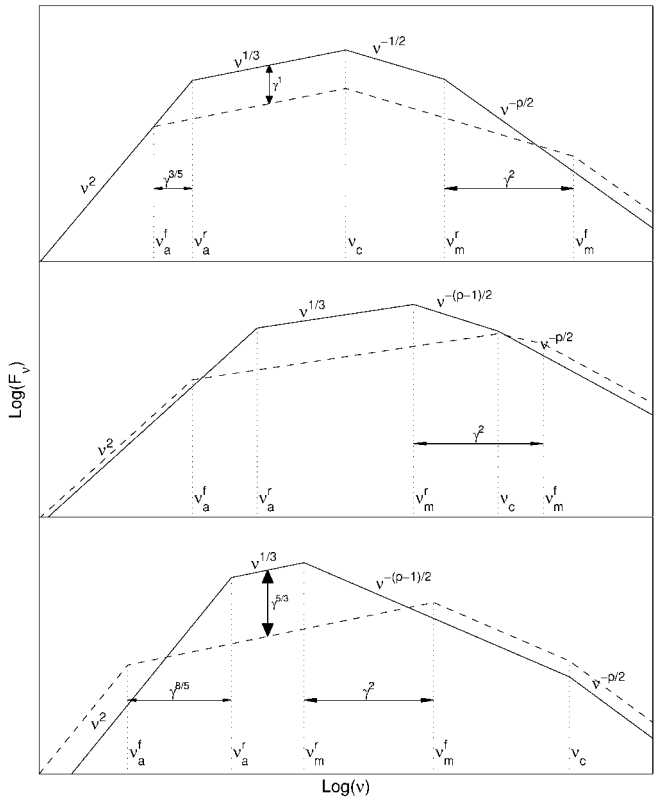

FIG. 1.—Spectrum of the reverse and forward shocks with synchrotron peaks at ν_m^r and ν_m^f, synchrotron self-absorption frequencies ν_a^r and ν_a^f, and cooling frequency ν_c (same for both, assuming $\epsilon_B^f = \epsilon_B^r$), for an electron injection spectrum proportional to γ^{-p}. *Top:* Both shocks fast cooling. *Middle:* Reverse slow, forward fast cooling. *Bottom:* Both slow cooling.

isfying

$$E_0(\gamma/\gamma_0)^{-s+1} \sim E \sim \gamma^2 R^3 \rho c^2. \tag{2}$$

If we assume that the outer density is $\rho \propto R^{-g}$ and use $t \sim R/\gamma^2 c$, we have

$$R = R_0(t/t_0)^{(1+s)/(7+s-2g)}, \tag{3}$$

$$\gamma = \gamma_0(t/t_0)^{-(3-g)/(7+s-2g)},$$

where R_0 and t_0 are the deceleration radius and deceleration time of the initial material with E_0 and γ_0. These scalings differ from those of Rees & Mészáros (1998), who obtained $s + 1$ where we have s in the expressions after our equation (2). For $s = 1$, the energy in the slow material adds up only logarithmically and therefore the above expression degenerates to the usual ones of instantaneous injection. However, for $s > 1$ where more energy is stored in a slowly moving material, we have a slower decay as more and more energy is added to the system as time evolves. These expressions are only valid for $g < 3$. Otherwise, the shocks are accelerating (see Blandford & McKee 1976 for $3 < g < 4$ and Best & Sari 2000 for $g > 4$). However, the most useful values of g are probably $g = 0$ and $g = 2$ (constant density or wind).

Since the additional slow shells catch up with the shocked material once these are with comparable Lorentz factors, the reverse shock is always mildly relativistic (Rees & Mészáros 1998; Kumar & Piran 1999). The thermal Lorentz factor of the electrons is therefore roughly given by the ratio of proton to electron mass, $\gamma_e^r \sim \epsilon_e m_p/m_e$. In the forward shock, the thermal Lorentz factor of the electrons is $\gamma_e^f \sim \epsilon_e \gamma m_p/m_e$.

The pressure behind the reverse shock is proportional to the density behind the reverse shock, which is comparable to the density in front of it (a mildly relativistic shock); therefore,

$$p_r \propto n_r \propto \frac{M}{R^3/\gamma} \propto t^{-(6+sg-g)/(7+s-2g)}.$$

As a check, we can see that this is also the pressure at the forward shock $p_f \propto \gamma^2 \rho$. The forward and reverse shock have the same bulk Lorentz factor and the same pressure, while the forward shock has a temperature that is higher by a factor of γ.

3. RADIATION

The dynamics above determine the bulk Lorentz factor and the thermal Lorentz factor of the electrons as function of time. To estimate the resulting synchrotron radiation, one also needs an estimate of the magnetic field. For a given magnetic field, the spectrum consists of four power-law segments separated by three break frequencies ν_a, ν_m, and ν_c (Sari, Piran, & Narayan 1998; Mészáros, Rees, & Wijers 1998). Adopting the standard assumption that the magnetic energy density is some fraction ϵ_B of equipartition, i.e., proportional to the pressure, we have $B \propto t^{-1/2(6+sg-g)(7+s-2g)}$. Since the pressure in the reverse and forward shock is identical, the magnetic field will also be the same if the equipartition parameter ϵ_B is the same. The difference between the forward and reverse shock lies then in the number of electrons (which is larger by a factor of γ at the reverse shock) and their thermal Lorentz factor (which is smaller by a factor of γ at the reverse shock). This results in the following properties, valid at any given moment:

1. The reverse shock peak flux is larger than that of the forward shock: $F_{\nu,\,\max}^r = \gamma F_{\nu,\,\max}^f$.
2. The typical frequency of the minimal electron in the reverse shock is smaller: $\nu_m^r = \nu_m^f/\gamma^2$.
3. The cooling frequency of the reverse and forward shock are equal: $\nu_c^r = \nu_c^f = \nu_c$.
4. At sufficiently early time (typically the first few weeks or months) $\nu_a^{r,f} < \nu_m^{r,f}$ and $\nu_a^{r,f} < \nu_c$. The self-absorption frequency of the reverse shock is larger than that of the forward shock. It is larger by a factor of $\gamma^{3/5}$ initially, when both are in fast cooling and by a factor of $\gamma^{8/5}$ if both are in slow cooling.

Points 1 and 2 above agree with those of Kumar & Piran, calculated for the discrete case. We have here generalized the result to include the effect of the cooling frequency and self-absorption frequency. The combined reverse + forward shock emission can therefore be one of three types, evolving in time in the following order:

a) Both reverse and forward shock are cooling fast: $\nu_a^f < \nu_a^r < \nu_c < \nu_m^r < \nu_m^f$.
b) Reverse is slow cooling, forward is fast cooling: $\nu_a^f < \nu_a^r < \nu_m^r < \nu_c < \nu_m^f$.
c) Both reverse and forward shock are in slow cooling: $\nu_a^f < \nu_a^r < \nu_m^r < \nu_m^f < \nu_c$.

These three spectra are presented in Figure 1. As evident from the figure, the forward shock dominates the emission at very low and very high frequencies, while the reverse shock contributes to a spectral "bump" at intermediate frequencies. The peak flux is that of the reverse rather than the forward shock. The combined spectrum is somewhat flatter than the usual one

TABLE 1

TEMPORAL EXPONENTS OF THE PEAK FREQUENCY ν_m, THE MAXIMUM FLUX F_{ν_m}, THE COOLING FREQUENCY ν_c, AND THE FLUX IN A GIVEN BANDWIDTH F_ν

				F_ν	
SHOCK	ν_m	F_{ν_m}	ν_c	$\nu_m < \nu < \nu_c$	$\nu > \max(\nu_c, \nu_m)$
F ……	$-\frac{24-7g+sg}{2(7+s-2g)}$	$\frac{6s-6+g-3sg}{2(7+s-2g)}$	$-\frac{4+4s-3g-3sg}{2(7+s-2g)}$	$-\frac{6-6s-g+3sg+\beta(24-7g+sg)}{2(7+s-2g)}$	$-\frac{-4-4s+g+sg+\beta(24-7g+sg)}{2(7+s-2g)}$
R ……	$-\frac{12-3g+sg}{2(7+s-2g)}$	$\frac{6s-12+3g-3sg}{2(7+s-2g)}$	$-\frac{4+4s-3g-3sg}{2(7+s-2g)}$	$-\frac{12-6s-3g+3sg+\beta(12-3g+sg)}{2(7+s-2g)}$	$-\frac{8-4s-3g+sg+\beta(12-3g+sg)}{2(7+s-2g)}$

NOTE.—F is forward, R is reverse. Calculated both in the adiabatic regime $\nu_m < \nu < \nu_c$ [$F_\nu \propto F_{\nu_m}(\nu_m/\nu)^\beta \propto t^{-\alpha}\nu^{-\beta}$, where $\beta = (p-1)/2$] and in the cooling regime $\nu_c < \nu_m < \nu$ [$F_\nu \propto (\nu_c/\nu_m)^{1/2}(\nu_m/\nu)^\beta \propto t^{-\alpha}\nu^{-\beta}$, where $\beta = p/2$].

(which uses the forward shock only). A good sampling of the spectrum, especially at low frequencies, can therefore show the existence or nonexistence of such a feature. The forward shock always dominates above $\nu > \max(\nu_m^f, \nu_c)$ by a small factor of γ^{p-2}. Since $p \cong 2$, the forward shock does not radiate much more than the reverse at high frequencies.

In the case of fast cooling, we have ignored the effect of the ordered structure of the electron's energy behind the shock (Granot, Piran, & Sari 2000), both for the reverse and forward shock. This effect will increase the emission at frequencies below the self-absorption frequency $\nu < \nu_a$, but will not change the qualitative conclusions of this Letter.

The spectrum displayed in Figure 1 is valid at any moment if the energy and momentum injection is continuous, but also at the moment of impact in the case of discrete injection. However, in the latter case the reverse shock component will rapidly disappear, as discussed by Sari & Piran (1999a, 1999b) and Mészáros & Rees (1999), and the forward shock after the collision will evolve as in the standard nonrefreshed scenario.

For the continuous case, the time dependence t^{-q} of the various quantities is given in Table 1, for arbitrary parameters s and g, assuming a spectral shape proportional to $\nu^{-\beta}$. Above the peak $\nu_{\max} = \min[\nu_m, \nu_c]$ where the flux has the value $F_{\nu,\max}$, the dependence $F_\nu \propto t^{-\alpha}\nu^{-\beta}$ is calculated separately for the slow and fast cooling regimes.

As a numerical example, we specialize to the constant density case, where $g = 0$. We then have

$$\nu_m^f = 2.0 \times 10^{13}\ \mathrm{Hz}\,(1+z)^{1/2} \times \epsilon_{B,-2}^{1/2}\epsilon_{e,0.5}^{2}E_{52}^{1/2}t_{\mathrm{day}}^{-3/2}\left(\frac{t}{t_0}\right)^{3(s-1)/2(7+s)}, \quad (4)$$

$$\nu_m^r = 9.1 \times 10^{11}\ \mathrm{Hz}\,(1+z)^{-1/4}\epsilon_{B,-2}^{1/2} \times \epsilon_{e,0.5}^{2}E_{52}^{1/4}n_0^{1/4}t_{\mathrm{day}}^{-3/4}\left(\frac{t}{t_0}\right)^{3(s-1)/4(7+s)}, \quad (5)$$

$$\nu_c = 2.7 \times 10^{15}\ \mathrm{Hz}\,(1+z)^{-1/2}\epsilon_{B,-2}^{-3/2} \times E_{52}^{-1/2}n_0^{-1}t_{\mathrm{day}}^{-1/2}\left(\frac{t}{t_0}\right)^{-3(s-1)/2(7+s)}, \quad (6)$$

$$F_{\nu,\max}^f = 2.6\ \mathrm{mJy}\ (1+z)\epsilon_{B,-2}^{1/2} \times E_{52}n_0^{1/2}D_{L,28}^{-2}\left(\frac{t}{t_0}\right)^{3(s-1)/(7+s)}, \quad (7)$$

$$F_{\nu,\max}^r = 12\ \mathrm{mJy}\ (1+z)^{11/8}\epsilon_{B,-2}^{1/2} \times E_{52}^{9/8}n_0^{3/8}D_{L,28}^{-2}t_{\mathrm{day}}^{-3/8}\left(\frac{t}{t_0}\right)^{27(s-1)/8(7+s)}. \quad (8)$$

For slow cooling, $\nu_c > \nu_m > \nu_a$, $\nu_{\max} = \nu_m$, and synchrotron self-absorption occurs at

$$\nu_a^f = 3.6\ \mathrm{GHz}\,(1+z)^{-1}\epsilon_{e,0.5}^{-1}\epsilon_{B,-2}^{1/5}E_{52}^{1/5}n_0^{3/5}\left(\frac{t}{t_0}\right)^{3/5(s-1)/(7+s)}, \quad (9)$$

$$\nu_a^r = 43\ \mathrm{GHz}\,(1+z)^{-2/5}\epsilon_{e,0.5}^{-1}\epsilon_{B,-2}^{1/5}E_{52}^{2/5}n_0^{2/5}t_{\mathrm{day}}^{-3/5}\left(\frac{t}{t_0}\right)^{6/5(s-1)/(7+s)}, \quad (10)$$

while for fast cooling, $\nu_m > \nu_c > \nu_{sa}$, the spectral peak is at $\nu_{\max} = \nu_c$, and we have

$$\nu_a^f = 0.3\ \mathrm{GHz}\,(1+z)^{-1/2}\epsilon_{B,-2}^{6/5}E_{52}^{7/10}n_0^{11/10}t_{\mathrm{day}}^{-1/2}\left(\frac{t}{t_0}\right)^{21(s-1)/10(7+s)}, \quad (11)$$

$$\nu_a^r = 0.8\ \mathrm{GHz}\,(1+z)^{-11/40}\epsilon_{B,-2}^{6/5} \times E_{52}^{31/40}n_0^{41/40}t_{\mathrm{day}}^{-29/40}\left(\frac{t}{t_0}\right)^{93(s-1)/40(7+s)}. \quad (12)$$

Using the normalization of the peak flux and the break points, the flux can be calculated at any frequency. Similar to the standard case, it is possible to test the model by comparing the temporal decay and spectral slopes. In the standard case (instantaneous injection), the flux above this frequency is falling with time, while the flux below this frequency is rising with time. The additional energy in the varying injection case tends to flatten the decay rate, and for high enough values of s can even make it grow (the t/t_0 factors in eqs. [5]–[12] are equivalent to a power of the ratio of the injected to initial energy E/E_0). Stated differently, one would need a steeper spectral index to give rise to the same observed temporal decay in the refreshed scenario. Table 2 summarizes for $g = 0$ the values of the spectral index β that can be inferred from a measured temporal decay index α in the instantaneous and refreshed scenarios, for reverse and forward shocks.

The spectral indices needed to explain a t^{-1} decay, as is observed in many bursts, are considerably steeper. Some confusion can occur between a slow cooling, moderately refreshed ($s = 2$) forward shock and a fast cooling forward shock in the nonrefreshed scenario, since these two scenarios predict a similar relation between α and β for nominal values. However, most other regimes are considerably different from the standard instantaneous forward shock prediction even if one only has moderately accurate spectral information.

TABLE 2
SPECTRAL INDICES β THAT WOULD BE DEDUCED FROM AN OBSERVED TEMPORAL DECAY INDEX α

		SPECTRAL INDEX β AS FUNCTION OF α ($F_\nu \propto t^{-\alpha}\nu^{-\beta}$)		
SHOCK	REGIME	No Injection	$s = 2$	$s = 3$
Forward	$\nu_m < \nu < \nu_c$	$2\alpha/3$ [2/3]	$(3\alpha + 1)/4$ [1]	$(5\alpha + 3)/6$ [4/3]
	$\nu > \max(\nu_m, \nu_c)$	$(2\alpha + 1)/3$ [1]	$(3\alpha + 2)/4$ [5/4]	$(5\alpha + 4)/6$ [3/2]
Reverse	$\nu_m < \nu < \nu_c$	Short-lived	$3\alpha/2$ [3/2]	$(10\alpha + 3)/6$ [13/6]
	$\nu > \max(\nu_m, \nu_c)$	Short-lived	$3\alpha/2$ [3/2]	$(5\alpha + 1)/3$ [2]

NOTE.—The third column gives the well-known "standard model" results for instantaneous injection for which the reverse shock does not last. The fourth and fifth columns are for continuous injection case with $s = 2$ and $s = 3$, respectively. For extended emission the reverse shock lives as long as the slower material keeps arriving, e.g., days. The values in brackets demonstrate the numerical value for a nominal temporal index of $\alpha = 1$.

4. DISCUSSION

The dynamics and emission of the forward and reverse shocks are controlled by several factors, including the continuity and nature of the energy and mass input, the possible existence of external density gradients, and the strength of the magnetic fields in these regions. A continuous injection of energy with a lower Lorentz factor has as its main consequence that it tends to flatten the decay slopes of the afterglow after it has gone through the maximum. An external density gradient (e.g., as in a wind with $\rho_{\rm ext} \propto r^{-g}$, where $g \sim 2$ might be typical) has the property of steepening the decay. This applies in general both to the forward and the reverse shocks.

We have suggested ways in which one can attempt to discriminate between the standard straight top-hat injection of energy and momentum with a single γ_0 and E_0, which then remains constant throughout the afterglow phase, and a refreshed scenario, in which the injection is also brief (e.g., comparable to the GRB duration and therefore instantaneous compared to the afterglow timescale) but in which there is a varying distribution of γ and of energy during that injection, so that matter ejected with low Lorentz factor catches up with the bulk of the flow on long timescales. The afterglow energy then increases with time. Under the simple assumption that both the forward and the reverse magnetic fields are equal ($\epsilon_{B,r} = \epsilon_{B,f}$), a remarkable prediction is that in all regimes (both shocks are fast cooling, reverse is slow cooling and forward shock is fast cooling, or both are slow cooling) the reverse shock spectrum joins seamlessly, or with only a very modest step $\propto \gamma^{p-2}$, onto the forward shock spectrum, extending it to lower frequencies. (This could be modified if, for instance, $\epsilon_{B,r} \ll \epsilon_{B,f}$, which would give a spectrum with a more pronounced step separating the reverse and forward components).

The afterglow of GRB 970508 showed a steep increase in the optical and X-ray fluxes between 1 and 2 days. This can be interpreted in terms of a varying injection event; e.g., Panaitescu, Mészáros, & Rees (1998) consider the radiation of the forward shock assuming a large value of s, a value of $\gamma_{\rm min} = 11 < \gamma < \gamma_0$, and a final energy $E_f = 3E_0$. After this time the energy is constant, and the afterglow can be fitted with a standard impulsive afterglow (e.g., Wijers & Galama 1999). How could we test the hypothesis that the "jump" between 0.5 and 2 days is indeed due to varying injection? A delayed energy injection (if ϵ_B is the same for the reverse and forward shocks) has a very strong prediction: we can estimate the forward shock break frequencies at $t = 2$ days by extrapolating them back from those at day 12, where the spectrum is well studied (e.g., Wijers & Galama 1999; Granot, Piran, & Sari 1999b). This results in $\nu_m^f \cong 1.3 \times 10^{12}$ Hz, $F_{\nu,\max} \sim 1.7$ mJy, $\nu_a^f \cong 3$ GHz, and $\gamma = 4$. Therefore, according to the lower frame of Figure 1, the reverse shock should have $\nu_m^r \cong 80$ and $\nu_a^r \cong 30$ GHz. The reverse shock signature is largest between these two frequencies, where the flux should exceed by an order of magnitude the simple extrapolation of the forward shock model back to day 2. At the more observationally accessible frequencies of 20 and 100 GHz, the flux increase due to the reverse shock should be 2.2 and 6 mJy, respectively. Unfortunately, the observations around 2 days at these frequencies were short and therefore of low sensitivity. The 3 σ upper limit of 6 mJy obtained by the Berkeley-Illinois-Maryland Association array is consistent with energy injection. This prediction of an additional low-frequency component in GRB 970508 is similar to that of Kumar & Piran (1999). However, taking the self-absorption frequency into account, we have shown here that this would not apply to the usually observed radio frequencies 1.4–8.4 GHz but to the range of 30–80 GHz. It is therefore of great value to obtain low-frequency observations or strong upper limits if such jumps in the optical and X-ray flux will be seen again in the future. If the reverse shock signature is not seen in other comparable bursts in which a light curve peak is detected at a certain time (1.5 days in this case), a varying injection episode can be ruled out as an explanation for this peak (unless $\epsilon_{B,r} \ll \epsilon_{B,f}$).

For GRB 990123b, a bright 9th magnitude optical flash was seen about 60 s after the trigger time (Akerlof et al. 1999), attributable to a reverse shock (Sari & Piran 1999a; Mészáros & Rees 1999) with an initial temporal decay $F \propto t^{-2}$, steeper than the subsequent decay $F \propto t^{-1.1}$ which is attributable to the forward shock. A standard impulsive injection fits better than a continuous one, since even a moderate injection ($s = 2$, $g = 0$) predicts a decay of $\alpha = 1$, while an impulsive event gives $\alpha = 2$, in good agreement with observations. (No spectral information was available for this burst in the first hour. We assumed conservatively $\beta = 1$ based on our accumulated knowledge from previous afterglows.)

For future GRB afterglow observations, the main prediction from having comparable values of ϵ_B in the forward and reverse shocks of baryon-loaded fireballs is that the peak flux is found at the peak frequency of the reverse, rather than of the forward shock, i.e., at lower frequencies than typically considered. The infrared, millimeter, and radio fluxes would therefore be expected to be significantly larger than for simple (forward shock) standard afterglow models (e.g., Fig 1). This holds whether the injection is continuous or discrete. The two contributions continue to evolve as a pair of smoothly joined components, the ratio of the two peak frequencies $\nu_m^r/\nu_m^f \propto \gamma^{-2}$ and peak fluxes $F_{\nu,\rm mr}/F_{\nu,\rm mf} \propto \gamma$ gradually approaching each other until they coincide at the transition to the nonrelativistic case $\gamma \sim 1$.

We are grateful to P. Kumar, A. Panaitescu, T. Piran, and M. J. Rees for comments. R. S. is supported by the Sherman Fairchild foundation. P. M. is supported through NASA NAG5-2857, the Guggenheim Foundation, the PMA Division, Astronomy Visitor Program and the Merle Kingsley fund at Caltech, and the Institute for Advanced Study.

REFERENCES

Akerlof, C., et al. 1999, Nature, 398, 400
Best, P., & Sari, R. 2000, Phys. Fluids, in press
Blandford, R. D., & McKee, C. 1976, Phys. Fluids, 19, 1130
Fenimore, E. E., & Ramirez-Ruiz, E. 1999, ApJ, submitted (astro-ph/9909299)
Galama, T., et al. 1999, Nature, 398, 394
Granot, J., Piran, T., & Sari, R. 1999a, ApJ, 513, 679
———. 1999b, ApJ, 527, 236
———. 2000, ApJ, 534, L163
Kumar, P., & Piran, T. 1999, preprint (astro-ph/9906002)
Mészáros, P., & Rees, M. J. 1999, MNRAS, 306, L39
Mészáros, P., Rees, M. J., & Wijers, R. 1998, ApJ, 499, 301
Panaitescu, A., Mészáros, P., & Rees, M. J. 1998, ApJ, 503, 314
Rees, M. J., & Mészáros, P. 1998, ApJ, 496, L1
Sari, R., & Piran, T. 1999a, ApJ, 520, 641
———. 1999b, ApJ, 517, L109
Sari, R., Piran, T., & Narayan, R. 1998, ApJ, 497, L17
Wijers, R. A. M. J., & Galama, T. 1999, ApJ, 523, 177